



Compressive properties of hollow lattice truss reinforced honeycombs (Honeytubes) by additive manufacturing: patterning and tube alignment

Jun Xu¹, Yaobo Wu¹, Lubing Wang, Jiani Li, Yuwei Yang, Yuli Tian, Zizheng Gong, Pinliang Zhang, Steven Nutt*, Sha Yin

M.C. Gill Composites Center, Department of Chemical Engineering and Materials Science, University of Southern California, 3651 Watt Way VHE-406, Los Angeles, CA 90089-0241, USA

* E-mail: nutt@usc.edu

Abstract: Honeytubes, a novel type of honeycomb formed by reinforcement with lattice trusses, were reported to exhibit enhanced buckling resistance. However, an in-depth analysis for the compressive performance and energy absorption capacity was lacking. In this paper, the effects of microstructure and tube alignment on compressive properties was studied. Four types of honeytubes were designed based on different topologies, geometries and tube patterns, and fabricated by selective laser sintering (SLS). Out-of-plane compression tests and finite element simulation were performed for the analysis. Results indicated that incorporation of lattice in honeycombs resulted in greater local strain in tubes and tube-rib connections. However, honeytubes exhibited superior energy absorption capability, even surpassing that of some metallic lattices. Balancing the configuration of tubes in honeytubes could ensure enhanced mechanical performance. This work demonstrates that materials designed by capitalizing on micro-topologies can regulate mechanical properties and provide insights for guiding the development of new materials.

Key words: Honeycomb; Honeytube; Lattice materials; Mechanical properties; Finite element analysis (FEA); Additive manufacturing;

Please cite the article as: J Xu, Y Wu, L Wang, J Li, Y Yang, Y Tian, Z Gong, P Zhang, S Nutt, and S Yin , “Compressive properties of hollow lattice truss reinforced honeycombs (honeytubes) by additive manufacturing: patterining and tube alignment effects” *Matls & Design* 156 (2018) 446-457 DOI: [10.1016/j.matdes.2018.07.019](https://doi.org/10.1016/j.matdes.2018.07.019)



1. INTRODUCTION

Lightweight material application and structural optimization design have become preferred routes for addressing increasingly stringent requirements for environmental and energy sustainability [1, 2]. Composite materials show superior specific properties compared to metallic counterparts, such as aluminum and steel, both of which are commonly used in ground vehicles, and are poised for entry into the automotive industry [3]. Additionally, micro-architected materials, which include ultra-lightweight periodic cellular materials, offer superior structural efficiency and multi-functional advantages because of the inherent open space. By adjusting micro-architecture, materials can be designed to achieve mechanical properties unattainable previously [4-7].

In recent decades, different design criteria have been used to develop architected materials with various topologies, including pyramidal lattice [3, 8-11], hollow pyramidal lattice [12, 13], and hierarchical lattices [14-16]. The hollow pyramidal lattice structure could be 4 times stronger than the corresponding solid truss counterparts at the same relative density [12]. In parallel, fabrication methods have been developed to produce different material systems, such as composite lattice [17], metallic lattice [18], and ceramic lattice [19], leading to unusual behavior under different loading conditions [20-24]. These studies have also shown that lattice materials have advantages in terms of specific properties and energy absorption capability compared with traditional lightweight materials.

Honeycombs are biomimetic cellular materials widely used in aerospace applications. The most common topologies are honeycomb with hexagonal microstructures, and triangular, square, Kagome honeycombs are also subsequently developed to satisfy more engineering demands [25, 26]. In recent years, honeycombs with novel structures have been proposed which exhibit interesting properties. Chiral honeycombs provide two distinct upper and lower bounds, which offer superior



transverse shear modulus in low weight application [27]. Hierarchy can be introduced into honeycombs which enhanced energy absorption ability due to the increase in the ratio of thickness to cell-edge length [28]. Honeycombs can exhibit negative Poisson's ratio after specific design, and their stiffness and energy absorption can be improved [29]. Inspired by the beetle elytron, a biologically-inspired prototype is introduced forming a new type of honeycomb by incorporating tubes into hexagonal honeycombs at vertices. The prototype exhibits enhanced mechanical properties and energy absorption capabilities [30]. Most recently, a new type of tube reinforced honeycombs, named as honeytubes, has been developed by the hybrid design of hollow pyramidal lattice and square honeycombs [31]. Like beetle elytron inspired honeycombs, honeytubes are composed of tubes and ribs, but the tubes are placed in the middle of ribs rather than at the vertices. Honeytubes exhibit enhanced buckling resistance and can be fabricated by slots interlocking or stereo lithography apparatus (SLA) [31]. However, the compressive performance and energy absorption capacity was not ever tested or simulated. Fundamental mechanisms responsible for the mechanical behavior of the hybrid designs remain to be examined.

To bridge this gap, honeytubes with different geometrical parameters and topologies are explored in this work to further examine specifically effects of rib patterns or tube alignment on compressive properties and guide structural design. First, all honeytubes and the corresponding honeycombs were fabricated by additive manufacturing and compressed through-thickness. Stiffness, strength and energy absorption capacities were measured, analyzed, and compared. Furthermore, finite element models were also validated and employed to assist analysis. Finally, effects of geometries, topologies, and tube patterns on compressive properties are considered and analyzed.

Please cite the article as: J Xu, Y Wu, L Wang, J Li, Y Yang, Y Tian, Z Gong, P Zhang, S Nutt, and S Yin ,
“Compressive properties of hollow lattice truss reinforced honeycombs (honeytubes) by additive manufacturing: patterning and tube alignment effects” *Matls & Design* 156 (2018) 446-457 DOI:
10.1016/j.matdes.2018.07.019



2. EXPERIMENTAL DETAILS

2.1. Design

The hybrid honeytube structures considered here feature combinations of square honeycomb and symmetrical pyramidal lattice tubes, as shown in Fig. 1. Fig. 1a shows an initial embodiment, a square honeytube denoted here as Sq_symtube ('Sq' means square shaped honeycombs; 'symtube' means symmetrically aligned hollow tubes). In a second embodiment, tube alignment was further simplified to be unidirectional, and those square honeytubes with unidirectional tubes in each strip were denoted as Sq_udtube ('Sq' means square shaped honeycombs; 'udtube' means unidirectionally aligned hollow tubes in each strip), as shown in Fig. 1b. Similarly, as shown in Fig. 1c-d, Kagome honeytube and triangular honeytube were also designed and denoted as Kag_udtube and Tri_udtube ('Kag' means Kagome shaped honeycombs while 'Tri' means triangular shaped honeycombs; 'udtube' is the same meaning as above defined), respectively. The relative densities of these structures, defined as the ratio of solid volume to that of a unit cell, were deduced as follows:

$$\bar{\rho} = \begin{cases} \left(\frac{2t}{l} - \frac{2dt}{l \sin \omega} \right) + \frac{\pi t(2d-t)}{2l \cos \omega}, & \text{for Sq_symtube or Sq_udtube} \\ \left(\frac{\sqrt{3}t}{l} - \frac{\sqrt{3}dt}{l \sin \omega} \right) + \frac{\sqrt{3}\pi t(2d-t)}{4l \cos \omega}, & \text{for Kag_udtube} \\ \left(\frac{2\sqrt{3}t}{l} - \frac{2\sqrt{3}dt}{l \sin \omega} \right) + \frac{\sqrt{3}\pi t(2d-t)}{2l \cos \omega}, & \text{for Tri_udtube} \end{cases} \quad (1)$$

where t and h are rib height and thickness in each strip; l is the grid length of honeycomb; d and ω are the outer diameter and inclination angle of tubes to the vertical plane in the honeycomb, while tube thickness in the present study is defined as one half of the ribs, equaling $t/2$.



2.2. Fabrication

Honeytubes were fabricated using selective laser sintering (SLS) additive manufacturing technology, capable of manufacturing materials with complex geometries without supporting structures, an important capability, since support structures are difficult to remove post-fabrication. The SLS printer uses a pulsed laser automatically scanning cross sections generated from a 3D model which describes the desired shapes, fusing powders together in the powder bed. The powder bed will be lowered after one cross-section is scanned, while a new layer of material will be applied on the top and then fused. The process is repeated until the designed object is totally created. Seven kinds of structures as designed above were printed, including honeytubes and their corresponding honeycombs, as shown in Figs. 2a-g. All the geometries are summarized in Table 1. The raw materials used here were commercialized PA3200 GF, a whitish, glass-filled polyamide 12 powder. Surfaces of the printed structures were examined with a microscope (Keyence VHX-6000) and SEM (HITACHI S-4800), as shown in Figs. 2h-j. The image (Fig. 2h) shows that the powders are sintered thoroughly, and the specimen shows slight local variability. The granules are distributed unevenly and pores between granules are present due to the insufficient delivered energy to the powder bed, as shown in Fig. 2i. Polyamide granules are relatively large, resulting in a rough surface, while glass granules are small with smooth surfaces fused to polyamide granules (Fig. 2j).

2.3. Compression

Out-of-plane quasi-static compression tests were performed on honeytubes, and compressive responses were analyzed and compared to those of honeycombs. All compression tests were performed (MTS 810 with load capacity of 100 kN) at a strain rate of $\sim 10^{-3}$ /s following ASTM



C365/C365M [26]. The compression force was read from the load cell, while displacement was measured using a laser extensometer. At least three repeated tests for each type of structure were performed to ensure the repeatability. Also, the compressive properties of parent materials were tested on glass reinforced polyamide cylinders (diameter of 12.7 mm and height of 25.4 mm) by bottom-up printing. The measured Young' modulus and strength was 1808 MPa and 45 MPa, respectively.

The out-of-plane compressive stress-strain curves are compared in Fig. 3 for three types of honeytubes, along with corresponding honeycombs, deformation history, and failure modes. The representative responses of the honeycombs were typical of cellular solids: the nominal stress increased almost linearly with the nominal strain, reached a peak value accompanied by rib buckling, then decreased with increasing compression until densification.

For Sq_symtube samples, two stress peaks occurred during compression, with deformation history and failure modes shown in Fig. 3b. The compressive stress increased linearly with strain, failed at the first peak by rib and tube buckling, then decreased as cracks initiated and propagated along tubes. However, the structure continued to bear load because of the strong coupling between ribs and tubes. After the first load drop, the compressive stress increased again and decreased after a second peak, caused by fracture at the rib-tube interface. Finally, the structure began to crush until densification ensued. For Tri_udtube samples, a similar compressive deformation behavior was observed, as shown in Figs. 3c-d. For Sq_udtube samples, a similar compressive behavior was observed, although the second stress peak was not as pronounced, (as the Sq_symtube sample), as shown in Fig. 3a. It was because the square honeytubes with unidirectional tubes were readily to slide as further compressed which was demonstrated in Fig. 3e. For Kag_udtube samples, the



compressive stress increased with strain followed by an extended plateau (without stress fluctuation) that was accompanied by buckling of tube and rib ends followed by structure sliding and densification, as shown in Figs. 3c and f.

In summary, honeytubes exhibited secondary enhancement after initial buckling because of the coupling effects of the lattice and honeycomb structures. The extended stress plateau (secondary enhancement) of honeytubes will promote energy absorption. However, incorporation of a lattice into honeycombs resulted in greater local strain in tubes, as well as stress concentration at the nodes between ribs and tubes, which slightly decreased the stiffness and strength of honeytubes.

3. NUMERICAL COMPUTATION

3.1. Method

Finite element (FE) simulation was carried out to analyze the compressive behavior and mechanisms of the different types of honeytubes. The FE models were developed (Abaqus platform) to investigate effects of topologies and geometric parameters on mechanical properties. The geometries of the models are summarized in Table. 2.

All simulations were performed on the same models as those in section 2.3, sandwiched between two rigid loading plates, as shown in Fig. 4a. The SOLID element C3D8R was selected for modeling honeytube cores, while the SHELL element S4R was used for loading plates using a discrete rigid surface. The mesh size was ~ 0.3 mm for honeytube cores and ~ 2 mm for compression plates, and thus each honeytube model included ~ 0.8 million solid elements in total.. The lower rigid plate was kept stationary, while the upper plate was allowed to translate by prescribing a displacement in the compression direction with other degrees of freedom constrained except out-of-plane displacement.

Please cite the article as: J Xu, Y Wu, L Wang, J Li, Y Yang, Y Tian, Z Gong, P Zhang, S Nutt, and S Yin ,
“Compressive properties of hollow lattice truss reinforced honeycombs (honeytubes) by additive manufacturing: patterining and tube alignment effects” *Matls & Design* 156 (2018) 446-457 DOI:
10.1016/j.matdes.2018.07.019



Additionally, two types of contacts were employed during the numerical analysis. For the honeytube or honeycomb cores, an automatic self-contact was adopted to simulate the contact between the deformed parts during deformation, while surface-to-surface frictional contact (friction coefficient $\mu = 0.2$) was employed between core and compression plates.

The complex contact conditions and nonlinear effects in the post-buckling period were accounted for in the code (Abaqus/Explicit). To balance time cost and simulation accuracy, pre-simulation was carried out to seek an appropriate compression speed and mass scaling factor. Among 20 groups of studies, a loading speed of 70 mm/s and mass scaling factor 1000 were selected and employed in all simulations. The kinetic energy of the FEA model was compared with the internal energy, as shown in Fig. 4b, and proved to be a small fraction of the latter, confirming the quasi-static condition.

3.2. Results

To validate the FE model, the compressive response of Sq_symtube and Sq_honeycomb was simulated and compared with experimental results, as shown in Fig. 5a. For Sq_symtubes, the tendency of the simulated curve duplicates the trends of experiments, but discrepancies exist. The linear stage from simulation results matches experiments, and the stiffness and strength can be accurately predicted by simulation. After the first stress peak, the stress drops by rib and tube buckling, followed by cracks propagated along tubes, as shown in Fig. 5b-c, until the second peak occurs. However, after the first peak, the simulated stress level is consistently greater than experiment, and the peak and valley are slightly delayed as well. Note that additive manufacturing usually introduces building defects, entrained porosity, and residual stress into fabricated structures [32], which result in additional discrepancies in simulated and experimental failure modes. Also, as honeytubes undergo large deformation, broken parts introduced by crushing begin to mutually



impinge, posing difficulties in simulation. Thus, the simulated post-buckling behavior for nylon-based structures is unlikely to accurately predict the observed compression process in all aspects. Meanwhile, for Sq_honeycomb, the simulated curve matches the experimental trends. The structure buckles first, followed by cracks appearing in the rib and at the connection area of each two ribs, as shown in Figs. 5d.

4. DISCUSSION

4.1. Geometrical Effects

The buckling resistance of hollow pyramidal lattice and honeycomb hybrids is inherently dependent on geometries due to strong constraining effects, as described previously [31]. Hence, the compressive properties of honeytubes in this study are not simple superpositions of hollow lattice and honeycombs. To evaluate the reinforcement effect of hollow lattice truss on compressive properties, honeytubes with different topologies and normalized geometries (t/l , d/l , ω) were simulated and compared with the corresponding honeycombs. Also, indexes $I1$ and $I2$ are employed to characterize the strengthening effect, and defined as the specific stiffness and strength of honeytubes, divided by that of the corresponding honeycombs. The variation of $I1$ and $I2$ with different normalized geometries are plotted in Fig. 6 and summarized below.

For tube inclination angle, the indices $I1$ and $I2$ increase with inclination angle ω , and the increasing rate decreases with ω , indicating that vertical tubes contribute more strongly to compressive properties. For tube slenderness ratio d/l , the index $I1$ continuously decreases with d/l , but the index $I2$ increases first, then decreases with d/l , indicating that an optimal d/l exists for



specific strength. This may be related to the failure mode transition of rib constrained tubes, representing that slender tubes of small d/l buckle along ribs while stubby tubes of large d/l tend to fail by fracture [31], which is difficult to accurately predict. As for t/l , I_1 and $I_2 < 1$ when $\omega = 45^\circ$ and $d/l = 0.133$, and vary slightly with t/l , indicating that t/l (associated with tube thickness) has little effect on mechanical behavior of honeytubes.

For different topologies, Sq_symtube generally exhibits the greatest reinforcement effect among the four types of honeytubes. The mechanical properties of Sq_symtube surpass those of corresponding honeycombs. Sq_symtube properties exceed those of Sq_udtube, and the tube alignment effect is addressed later. Although Tri_udtube possesses the greatest stiffness and strength values with the same geometry, as shown previously, the strengthening effect is not the maximum, as indicated from I_1 and I_2 of Tri_udtube in Fig. 6. In contrast, Kag_udtube exhibits the least strengthening compared with the corresponding honeycombs.

The specific stiffness and strength values of honeytubes are plotted in an Ashby Chart in Fig. 12a. Although the mechanical properties of honeytubes are inferior to that of some honeycombs, they still exhibit their distinct advantages over polymer foam, biomaterials [3, 33] and other lightweight cellular materials [34, 35], which makes them potential lightweight candidates.

4.2. Effects of Tube Alignment In Each Strip

4.2.1 Comparisons between Sq_udtube and Sq_symtube

The mechanical performance of Sq_udtube and Sq_symtube with different normalized geometries d/l and tube inclination angles ω are simulated with fixed $t/l = 0.5$ and compared, as shown in Fig. 7. The stiffness values of Sq_udtube and Sq_symtube vary slightly with d/l , while the strength increases initially, then decreases with d/l . Both stiffness and strength of Sq_symtube and



Sq_udtube increase continuously with inclination angle ω . Moreover, the stiffness and strength values of Sq_symtube are always greater than those of Sq_udtube samples for any specific d/l and inclination angle ω , which is attributed to the slide phenomenon described in section 2.3.

4.2.2 Effect of degree-of-freedom allowing sliding on compressive properties

Different constraint conditions between Sq_udtube and loading plates were employed to study the effects of the slide phenomenon on compressive properties. Three different surface-to-surface contact friction coefficients were applied to the same FE model, and the corresponding compressive responses were compared, shown in Fig. 8a. Note that different contact friction coefficients represent different interfacial properties between cores and plates of a sandwich structure. As the friction coefficient μ is set to zero, the compressive strength of Sq_udtube decreases comparing to $\mu = 0.2$ and $\mu = 1$. Setting $\mu = 1$ means the honeytube cores are fully tied with facesheets and cannot slide over each other, and thus compressive strength increases, and the compressive properties of Sq_udtube are comparable to those of Sq_symtube. In addition, Fig.8b shows the in-plane shear stress data of Sq_udtube for three friction coefficients. As the slide of Sq_udtube is totally restricted ($\mu = 1$), and greater shear stress level is observed, as shown in Fig. 8b(i). In contrast, as $\mu = 0.2$ or $\mu = 0$, shear stress values are much lower, and the shear stress states are shown in Figs. 8b(ii) and (iii). Sq_symtube is insensitive to boundary constraints because the slide phenomenon is not observed during experiments and simulation. The insensitivity arises because Sq_symtube contains symmetrical tubes, which induce no slide and shear stress much less than compression (Fig. 8c). These results indicate that different tube alignments will introduce different stress states. Furthermore, unbalanced tube arrangements in each strip will cause the structural slide phenomenon, which finally decreases the load bearing capacity in compression. However, when used as sandwich



cores with ideally bonded facesheet-core interfaces, core slide will not occur, and the compressive behavior should resemble that of Sq_symtube, although the high-level shear stress at the interface will affect the interfacial reliability and affect mechanical properties.

4.3 Effects of Strip Pattern

To further explore the effects of tube arrangements on compressive behavior of honeytubes, Sq_udtubes with different strip patterns were designed. The Sq_udtube in Fig. 9a contains ten strips in total, with five in the x-direction and five in the z-direction. We assume that the structure is axisymmetric about x and z axes, and strips in the x-direction are obtained by rotating those in the z-direction by 90 degrees. Thus, the pattern of Sq_udtube can be determined by three independent strips, as indicated in Fig. 9a. Considering the middle strip as the reference (marked as 1), those in which tubes are aligned in the same direction are marked as 1, while opposites as 0. Four combinations exist, termed as 111, 110, 101, 100 shown in Fig. 9b. Note that the 111 pattern is the specimen studied in experiments.

Sq_udtubes with four different patterns are simulated and compared with Sq_symtubes, as shown in Fig. 10. To quantify the slide phenomenon of Sq_udtubes, the upper and lower loading plates are tied to the honeytubes, and the loading plate can move only along the compression direction, with other degrees of freedom free (equal to the boundary condition of $\mu = 0$ in section 4.2.2). The upper plates of honeytubes (blue line) offset from the original position as compressed, and different patterned honeytubes exhibit different offset distances, as shown in Fig. 10a-b. Fig. 10b reveals that Sq_udtubes (111) exhibits the maximum offset displacement, while Sq_udtubes (101) exhibit the minimum, and the Sq_symtube is near zero.



The compressive force-displacement curves of different patterned honeytubes, shown in Fig. 10c, indicate that Sq_udtubes (101) exhibit compressive behavior similar to that of the Sq_symtube, while Sq_udtubes (111) exhibit the lowest performance levels. The results demonstrate that honeytubes with balanced patterns and tube arrangements possess superior compressive performance and less slide behavior relative to unbalanced patterns.

4.3 Energy Absorption Capability

Energy absorption (EA) capacity is defined as the energy dissipated during the crushing process, and is obtained from the area under the force-displacement curve as $W = \int_0^{d_D} F d\delta$, where $\varepsilon_D = d_D/h$ is the densification strain. Specific energy absorption (SEA) is the energy dissipated W divided by structural mass m and given by $SEA = W/m$. An energy-absorption efficiency approach [36] is proposed to calculate the densification strain when

$$\left. \frac{d\Psi(\varepsilon)}{d\varepsilon} \right|_{\varepsilon=\varepsilon_D} = 0 \quad (2)$$

where the efficiency parameter, Ψ , is defined as the absorbed energy per unit volume up to a given nominal strain divided by the corresponding stress value and given by $\Psi = \int_0^\varepsilon \sigma(\varepsilon) d\varepsilon / \sigma(\varepsilon)$. The variation of Ψ for honeytubes is plotted in Fig. 11a with a corresponding stress-strain curve, and the densification strain is corresponding to the maximum efficiency.

SEA of honeytubes was performed using the experimental compressive curves, then compared with the corresponding honeycombs, as shown in Fig. 11b. For samples of Sq_symtube, Kag_udtube and Tri_udtube, SEA values are significantly greater than their corresponding honeycombs, demonstrating that the enhanced coupling behavior between tubes and ribs, combined with tube fracture during compressing, dissipates additional energy. However, for Sq_udtubes, SEA



values are the lowest among all structures due to the severe slide behavior during compression, discussed previously. SEA of honeytubes versus specific strength is plotted in Fig. 12b and compared with that of the corresponding honeycombs and other lightweight cellular materials [33, 37-39]. Honeytubes exhibit superior energy absorption capability relative to polymer honeycombs produced by additive manufacturing, Luffa sponge [33], aluminum foam [37] and even metallic lattice materials [38].

5. CONCLUSIONS

Hollow lattice truss-reinforced honeycombs, termed honeytubes, were designed by combining the microstructures of hollow lattices and honeycombs in three geometrical configurations. Honeytubes and the corresponding honeycombs were fabricated by additive manufacturing (Selective Laser Sintering) using glass-reinforced nylon particles. The uni-axial compressive properties were analyzed experimentally and computationally, yielding the following results:

- Strain hardening behavior (two stress peaks or extended plateaus) was observed during compressive loading of honeytubes. The structures exhibited enhanced energy absorption capability relative to corresponding honeycombs and other lightweight materials. However, the measured stiffness and strength values of honeytubes were less than those of corresponding honeycombs, due to the increased local strain in tubes and stress concentration at the rib-tube nodes after introducing hollow trusses.
- The specific properties of honeytubes depended on geometrical parameters and topologies, and were validated by simulation models. The strengthening effect sequence for different types of



honeytubes relative to corresponding honeycombs was: $Sq_symtube > Tri_udtube > Sq_udtube > Kag_udtube$.

- The effects of tube alignment and strip patterns were analyzed, revealing that $Sq_symtube$ outperformed Sq_udtube because Sq_udtube was able to slide during compression loading due to the asymmetrical tubes in each strip. However, when slide was fully constrained by setting fixed boundary conditions, Sq_udtube possessed exhibited mechanical properties identical to $Sq_symtube$. However, the high level shear stress levels in $Sq_udtubes$ will reduce sandwich core-facesheet interfacial reliability in engineering applications. In addition, banlanced configurations exhibited mechanical properties comparable to $Sq_symtubes$, ensuring enhancement of mechanical properties of honeytubes.

Honeytubes produced by hybridizing microstructures provide opportunities to tailor mechanical properties of lightweight materials and to optimize energy absorption abilities for crash protection. Such structures expand materials selection options to spaces in materials property charts that are presently vacant. These results provide guidelines for designing hybrid materials and producing promising candidates for weight-critical engineering applications.

Acknowledgements: This work was financially supported by the National Natural Science Foundation of China under grant No. U1664250, the National Key Research and Development Program of China (2017YFB0103703), the Fundamental Research Funds for the Central Universities, Beihang University, CAST-BISEE2017-021, Young Elite Scientist Sponsorship Program by CAST, and Opening fund of State Key Laboratory for Strength and Vibration of Mechanical Structures, Xi'an Jiaotong University (SV2016-KF-20).

Please cite the article as: J Xu, Y Wu, L Wang, J Li, Y Yang, Y Tian, Z Gong, P Zhang, S Nutt, and S Yin ,
“Compressive properties of hollow lattice truss reinforced honeycombs (honeytubes) by additive manufacturing: patterining and tube alignment effects” *Matls & Design* 156 (2018) 446-457 DOI:
10.1016/j.matdes.2018.07.019



References:

- [1] M.F. Ashby, Y.J.M. Bréchet. Designing hybrid materials. *Acta Mater* 2003; 51: 2801-5821.
- [2] X. Cui, H. Zhang, S. Wang, L. Zhang, J. Ko. Design of lightweight multi-material automotive bodies using new material performance indices of thin-walled beams for the material selection with crashworthiness consideration. *Mater Design* 2011; 32: 815-821.
- [3] J. Xu, X. Gao, C. Zhang, and S. Yin. Flax fiber-reinforced composite lattice cores: A low-cost and recyclable approach. *Mater Design* 2017; 133: 444-454.
- [4] T.A. Schaedler, A.J. Jacobsen, A. Torrents, A.E. Sorensen, J. Lian, J.R. Greer, L. Valdevit and W.B. Varter. Ultralight Metallic Microlattices. *Science* 2011; 334(6058): 962-965.
- [5] X. Zheng, H. Lee, T.H. Weisgraber, M. Shusteff, J. Deotte, E.B. Duoss, et al. Ultralight, ultrastiff mechanical metamaterials. *Science* 2014; 344(6190): 1373-1377.
- [6] T. Li, X. Hu, Y. Chen, and L. Wang. Harnessing out-of-plane deformation to design 3D architected lattice metamaterials with tunable Poisson's ratio. *Sci Rep* 2017; 7(1).
- [7] J. Hu, S. Yin, T.X. Yu, and J. Xu. Dynamic compressive behavior of woven flax-epoxy-laminated composites. *Int J Impact Eng* 2018; 117: 63-74.
- [8] J. Xiong, R. Ghosh, L. Ma, A. Vaziri, Y. Wang, and L. Wu. Sandwich-walled cylindrical shells with lightweight metallic lattice truss cores and carbon fiber-reinforced composite face sheets. *Compos Part A-appl S* 2014; 56: 226-238.
- [9] J. Liu, L. Xiang, and T. Kan. The effect of temperature on the bending properties and failure mechanism of composite truss core sandwich structures. *Compos Part A-appl S* 2015; 79: 146-154.
- [10] B. Wang, L. Wu, L. Ma, Y. Sun, and S. Du. Mechanical behavior of the sandwich structures with carbon fiber-reinforced pyramidal lattice truss core. *Mater Design* 2010; 31(5): 2659-2663.
- [11] M. Li, L. Wu, L. Ma, B. Wang, and Z. Guan. Mechanical Response of All-composite Pyramidal Lattice Truss Core Sandwich Structures. *J Mater Sci Technol* 2011; 27(6): 570-576.
- [12] S. Yin, L. Wu, L. Ma, and S. Nutt. Pyramidal lattice sandwich structures with hollow composite trusses. *Compos Struct* 2011; 93(12): 3104-3111.
- [13] K.J. Maloney, C.S. Roper, A.J. Jacobsen, W.B. Carter, L. Valdevit, and T.A. Schaedler. Microlattices as architected thin films: Analysis of mechanical properties and high strain elastic recovery. *Apl Materials* 2013; 1(2).
- [14] F. Sun, C. Lai, H. Fan, and D. Fang. Crushing mechanism of hierarchical lattice structure. *Mech Mater* 2016; 97: 164-183.
- [15] Y. Chen, Z. Jia, and L. Wang. Hierarchical honeycomb lattice metamaterials with improved thermal resistance and mechanical properties. *Compos Struct* 2016; 152: 395-402.
- [16] X. Zheng, R. Zheng, W. Smith, J. Jackson, B. Moran, and H. Cui. Multiscale metallic metamaterials. *Nat Mater* 2016; 15(10): 1100.
- [17] C. Schneider, M.N. Velea, S. Kazemahvazi, and D. Zenkert. Compression properties of novel thermoplastic carbon fibre and poly-ethylene terephthalate fibre composite lattice structures. *Mater Des* 2015; 65: 1110-1120.

Please cite the article as: J Xu, Y Wu, L Wang, J Li, Y Yang, Y Tian, Z Gong, P Zhang, S Nutt, and S Yin ,
“Compressive properties of hollow lattice truss reinforced honeycombs (honeytubes) by additive
manufacturing: patterining and tube alignment effects” *Matls & Design* 156 (2018) 446-457 DOI:
10.1016/j.matdes.2018.07.019



- [18] L. Dong, V. Deshpande, and H. Wadley. Mechanical response of Ti-6Al-4V octet-truss lattice structures. *Int J Solids Struct* 2015; 60-61: 107-124.
- [19] F. Yang, S. Cheng, T. Zeng, Z.H. Wang, G.D. Xu, J. Zhai, and D. Fang. Mechanical and oxidation properties of C/SiC corrugated lattice core composite sandwich panels. *Compos Struct* 2016; 158: 137-143.
- [20] Y.L. Liu, T.A. Schaedler, and X. Chen. Dynamic energy absorption characteristics of hollow microlattice structures. *Mech Mater* 2014; 77: 1-13.
- [21] J.M. Hundley, E.C. Clough, and A.J. Jacobsen. The low velocity impact response of sandwich panels with lattice core reinforcement. *Int J Impact Eng* 2015; 84: 64-77.
- [22] S. Yin, A.J. Jacobsen, L. Wu, and S.R. Nutt. Inertial stabilization of flexible polymer microlattice materials. *J Mater Sci* 2013; 48(19): 6558-6566.
- [23] J. Zhang, Q. Qin, C. Xiang, Z. Wang, and T.J. Wang. A theoretical study of low-velocity impact of geometrically asymmetric sandwich beams. *Int J Impact Eng* 2016; 96: 35-49.
- [24] J. Zhang, Q. Qin, and T.J. Wang. Compressive strengths and dynamic response of corrugated metal sandwich plates with unfilled and foam-filled sinusoidal plate cores. *Acta Mech* 2013; 224(4): 759-775.
- [25] W. Miller, C.W. Smith, F. Scarpa, and K.E. Evans. Flatwise buckling optimization of hexachiral and tetrachiral honeycombs. *Compos Sci Technol* 2010; 70(7): 1049-1056.
- [26] F. Scarpa, S. Blain, T. Lew, D. Perrott, M. Ruzzene, and J.R. Yates. Elastic buckling of hexagonal chiral cell honeycombs. *Compos Part A-appl S* 2007; 38(2): 280-289.
- [27] A. Lorato, P. Innocenti, F. Scarpa, A. Alderson, K.L. Alderson, K.M. Zied, N. Ravirala, W. Miller, C.W. Smith, and K.E. Evans. The transverse elastic properties of chiral honeycombs. *Compos Sci Technol* 2010; 70(7): 1057-1063.
- [28] J. Fang, G. Sun, N. Qiu, T. Pang, S. Li, and Q. Li. On hierarchical honeycombs under out-of-plane crushing. *Int J Solids Struct* 2018; 135: 1-13.
- [29] T. Li, Y. Chen, X. Hu, Y. Li, and L. Wang. Exploiting negative Poisson's ratio to design 3D-printed composites with enhanced mechanical properties. *Mater Design* 2018; 142: 247-258.
- [30] X. Zhang, J. Xie, J. Chen, Y. Okabe, L. Pan, and M. Xu. The beetle elytron plate: a lightweight, high-strength and buffering functional-structural bionic material. *Sci Rep* 2017; 7(1).
- [31] S. Yin, J. Li, B. Liu, K. Meng, Y. Huan, S.R. Nutt, and J. Xu. Honeytubes: Hollow lattice truss reinforced honeycombs for crushing protection. *Compos Struct* 2017; 160: 1147-1154.
- [32] A.S. Wu, D.W. Brown, M. Kumar, G.F. Gallegos, and W.E. King. An Experimental Investigation into Additive Manufacturing-Induced Residual Stresses in 316L Stainless Steel. *Metall Mater Trans A* 2014; 45(13): 6260-6270.
- [33] J. Shen, Y. Xie, X. Huang, S. Zhou, and D. Ruan. Mechanical properties of luffa sponge. *J Mech Behav Biomed Mater* 2012; 15: 141-152.
- [34] D.W. Abueidda, M. Bakir, R.K.A. Al-Rub, J.S. Bergström, N.A. Sobh, and I. Jasiuk. Mechanical properties of 3D printed polymeric cellular materials with triply periodic minimal surface architectures. *Mater Design* 2017; 122: 255-267.
- [35] X. Ren, J. Shen, P. Tran, T. D. Ngo, and Y. Xie. Design and characterisation of a tuneable 3D buckling-induced auxetic metamaterial. *Mater Design* 2018; 139: 336-342.
- [36] M. Avallé, G. Belingardi, and R. Montanini. Characterization of polymeric structural foams under compressive impact loading by means of energy-absorption diagram. *Int J Impact Eng* 2001; 25: 455-472.

Please cite the article as: J Xu, Y Wu, L Wang, J Li, Y Yang, Y Tian, Z Gong, P Zhang, S Nutt, and S Yin ,
“Compressive properties of hollow lattice truss reinforced honeycombs (honeytubes) by additive
manufacturing: patterining and tube alignment effects” *Matls & Design* 156 (2018) 446-457 DOI:
10.1016/j.matdes.2018.07.019



- [37] I. Duarte, M. Vesenjak, and L. Krstulović-Opara. Compressive behaviour of unconstrained and constrained integral-skin closed-cell aluminium foam. *Compos Struct* 2016; 154: 231-238.
- [38] F. Cote, V.S. Deshpande, N.A. Fleck, and A.G. Evans. The compressive and shear responses of corrugated and diamond lattice materials. *Int J Solids Struct* 2006; 43: 6220-6242.
- [39] S. Yin, L. Wu, L. Ma, and S. Nutt. Hybrid truss concepts for carbon fiber composite pyramidal lattice structures. *Compos Part B-Eng* 2012; 43(4): 1749-1755.



Figure Captions

Figure 1. Illustrations for four types of honeytubes: a) Sq_symtube, b) Sq_udtube, c) Kag_udtube, d) Tri_udtube, with i) 3D view, ii) top view and iii) representative unit cell of these honeytube structures.

Figure 2. Specimens fabricated by selective laser sintering: a) Sq_honeycomb; b) Kag_honeycomb; c) Tri_honeycomb; d) Sq_symtube; e) Sq_udtube; f) Kag_udtube; g) Tri_udtube; h) rough surfaces of the printed structures; i) SEM image indicating the distribution of glass and polyamide granules with j) the enlarged figure showing that a single glass granule attached to the polyamide one.

Figure 3. a) Compressive stress-strain curves of Sq_udtube, and Sq_symtube comparing with those of Sq_honeycomb; b) deformation history of Sq_symtube; c) compressive responses of Kag_udtube and Tri_udtube comparing with those of the corresponding honeycombs; d) failure modes of Tri_udtube and Kag_udtube; the slide phenomenon of e) Sq_udtube and f) Kag_udtube during compression.

Figure 4. a) Illustration of the simulation model; b) variations of the kinetic energy and internal energy with time.

Figure 5. a) Comparison of compressive stress-strain curves between experimental and simulation results for Sq_symtube and Sq_honeycomb; b) stress distribution contour of Sq_symtube with c) the partial enlargement figure showing failure mode and fracture area comparing with experimental result; d) failure mode of Sq_honeycomb at $\varepsilon = 0.20$ during compression and compared with the corresponding simulation results.

Figure 6. Variation of strengthening index I_1 and I_2 with geometries a) ω , b) d/l and c) t/l for different types of honeytubes.

Figure 7. Comparisons of a) stiffness and b) strength between Sq_symtube and Sq_udtube at different d/l and inclination angle ω .

Figure 8. a) Compressive curves of Sq_symtube and Sq_udtube under different friction coefficients; b) transverse shear stress distribution of Sq_udtube under friction coefficient (i) $\mu = 1$, (ii) $\mu = 0.2$ and (iii) $\mu = 0$; c) transverse shear stress distribution of Sq_symtube under friction coefficient (i) $\mu = 0.2$ and (ii) $\mu = 0$.

Figure 9. Illustration of a) the independent design variables for Sq_udtube and the reference strip and b) four different strip patterns.

Figure 10. a) Illustrations of slide displacement of honeytubes with five different patterns as compressed; b) variations of transverse displacement of upper plates versus compressive displacement; c) force-displacement curves of Sq_udtubes with various tube patterns comparing with Sq_symtube.

Figure 11. a) Calculation of the densification strain; b) specific energy absorption of honeytubes with different topologies comparing with the corresponding honeycombs.

Figure 12. a) Specific stiffness plotted against specific strength, and b) specific energy absorption plotted against specific strength of honeytubes comparing with other lightweight cellular materials.

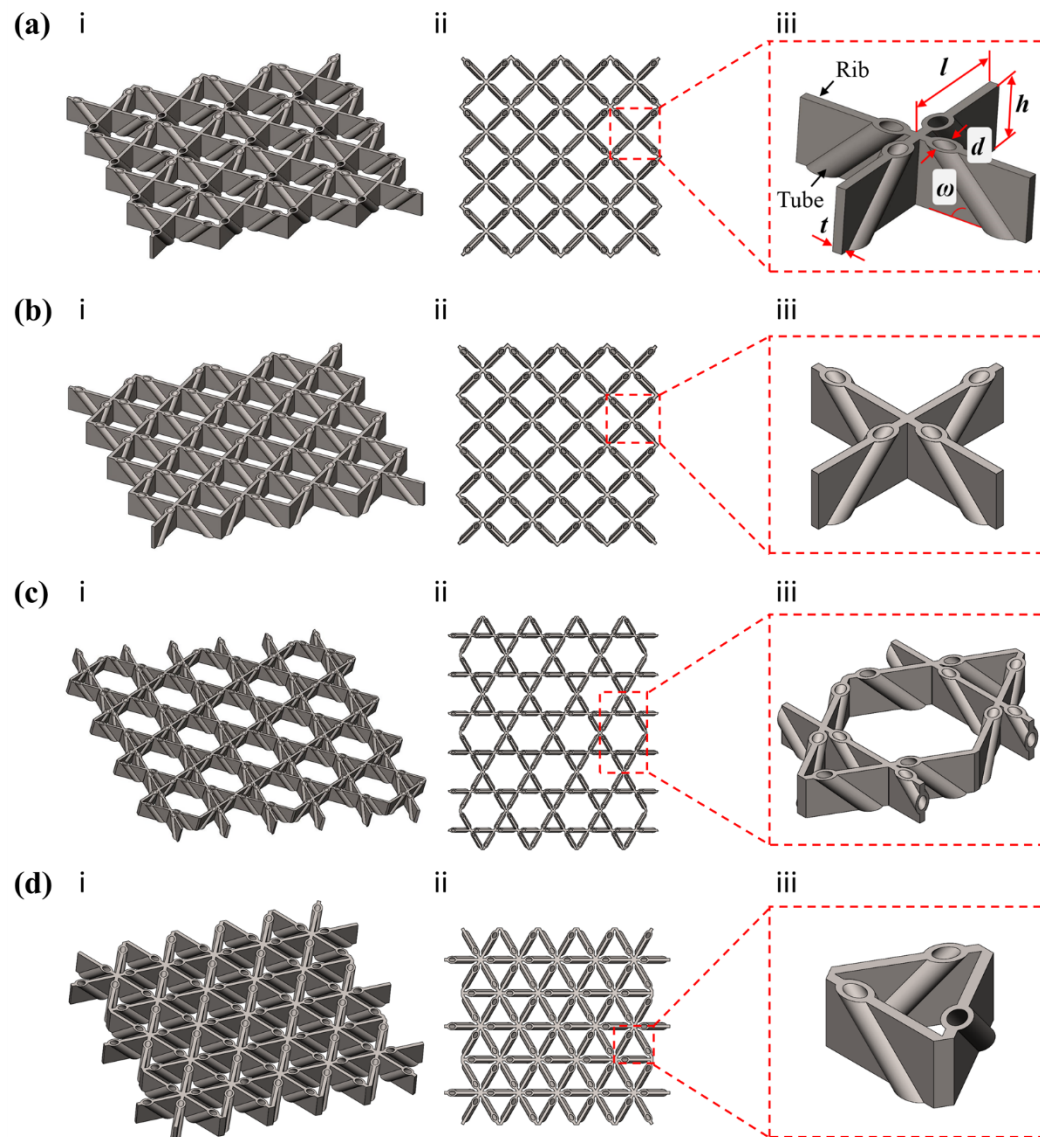


Figure 1

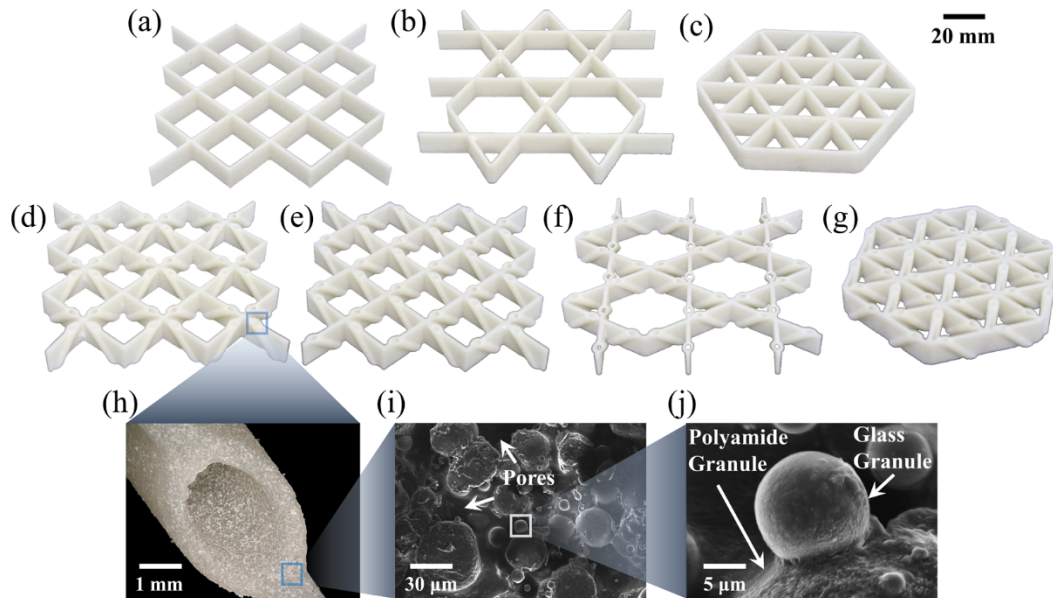


Figure 2

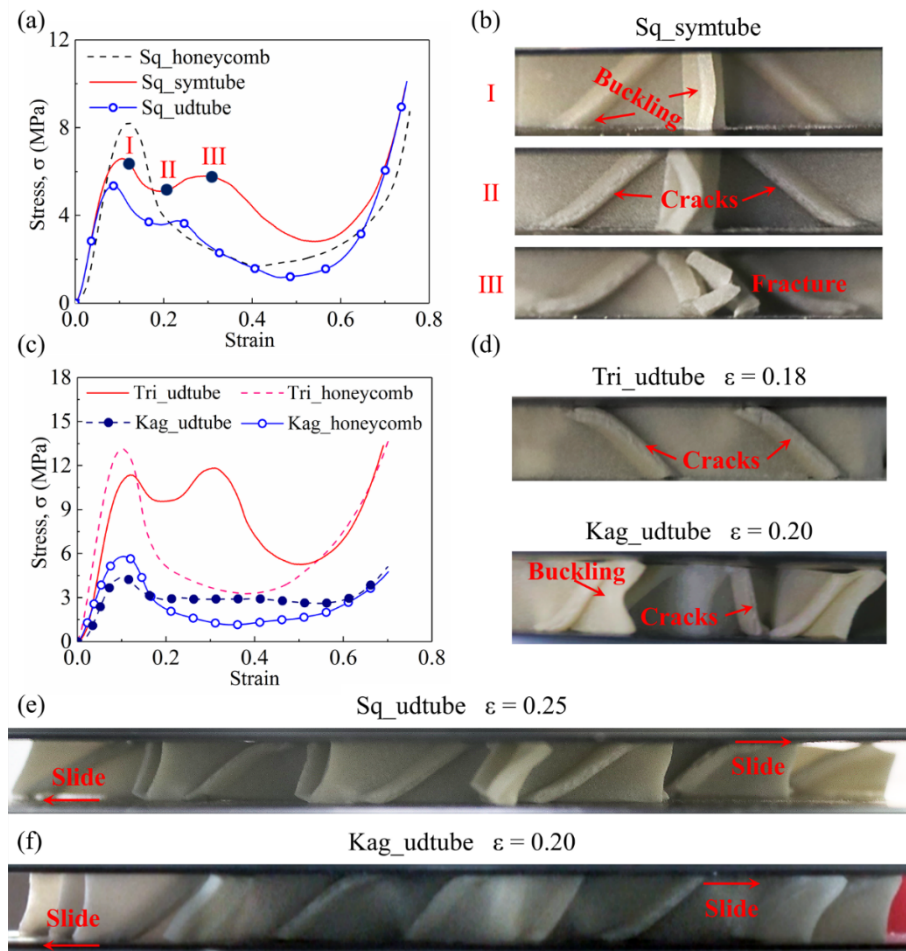


Figure 3

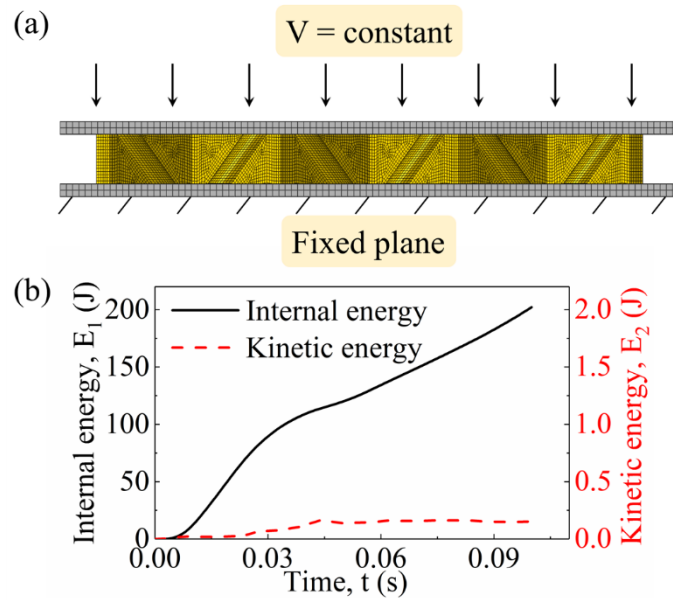


Figure 4.

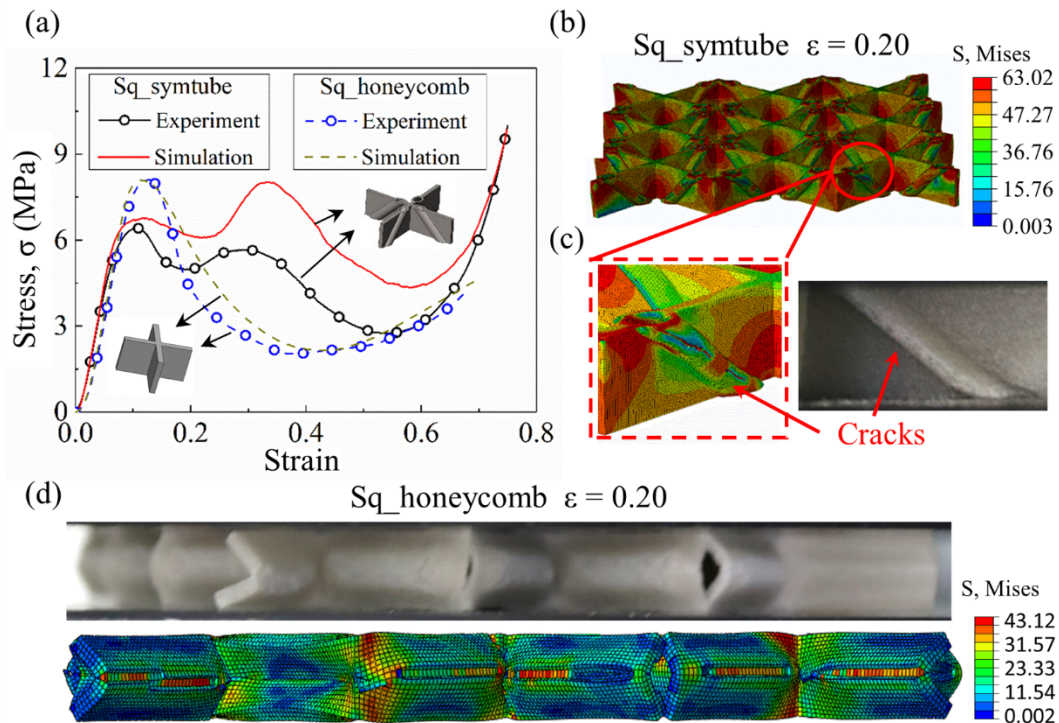


Figure 5

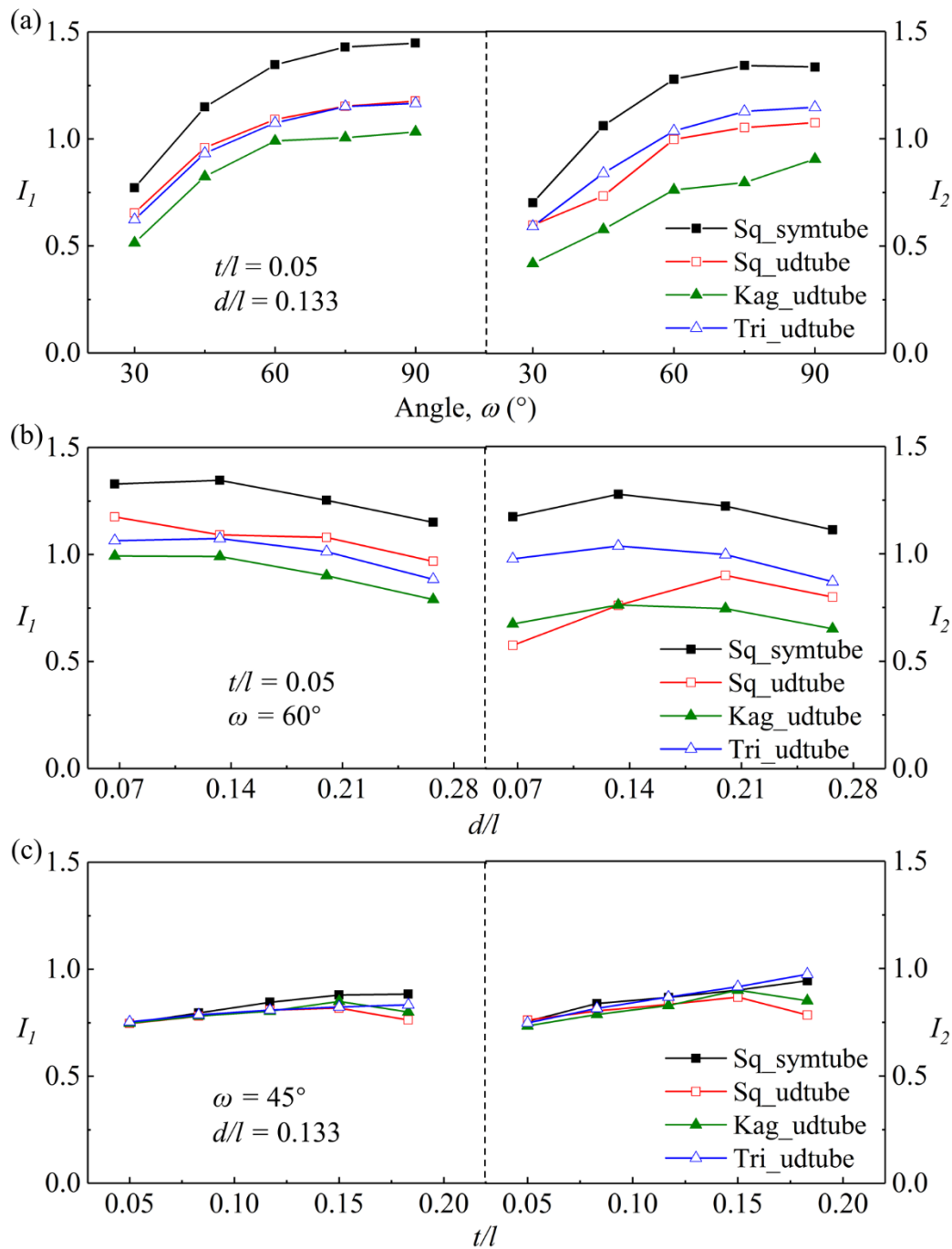


Figure 6

Please cite the article as: J Xu, Y Wu, L Wang, J Li, Y Yang, Y Tian, Z Gong, P Zhang, S Nutt, and S Yin ,
**“Compressive properties of hollow lattice truss reinforced honeycombs (honeytubes) by additive
 manufacturing: patterning and tube alignment effects”** *Matls & Design* 156 (2018) 446-457 DOI:
 10.1016/j.matdes.2018.07.019

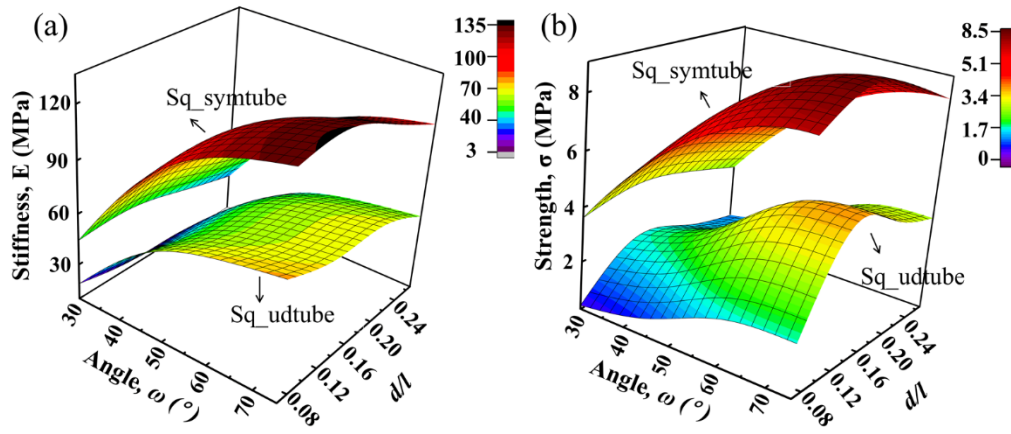


Figure 7

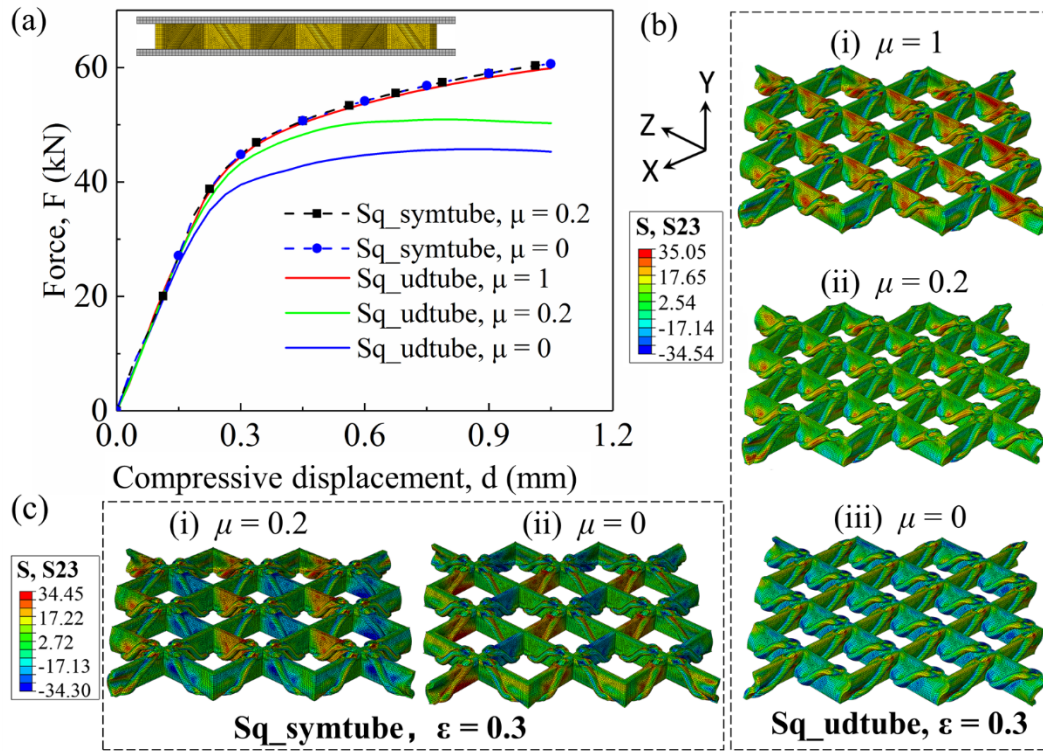


Figure 8

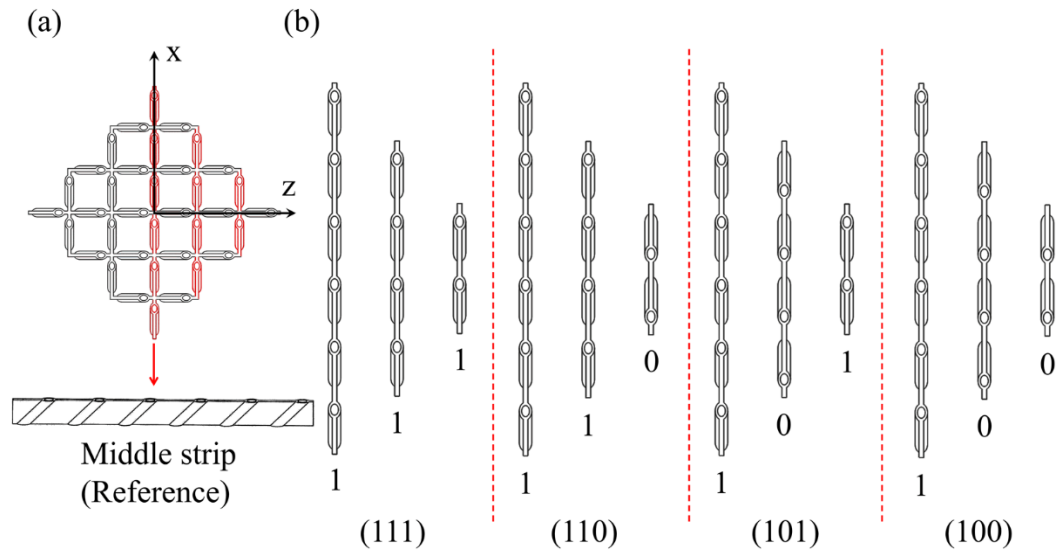
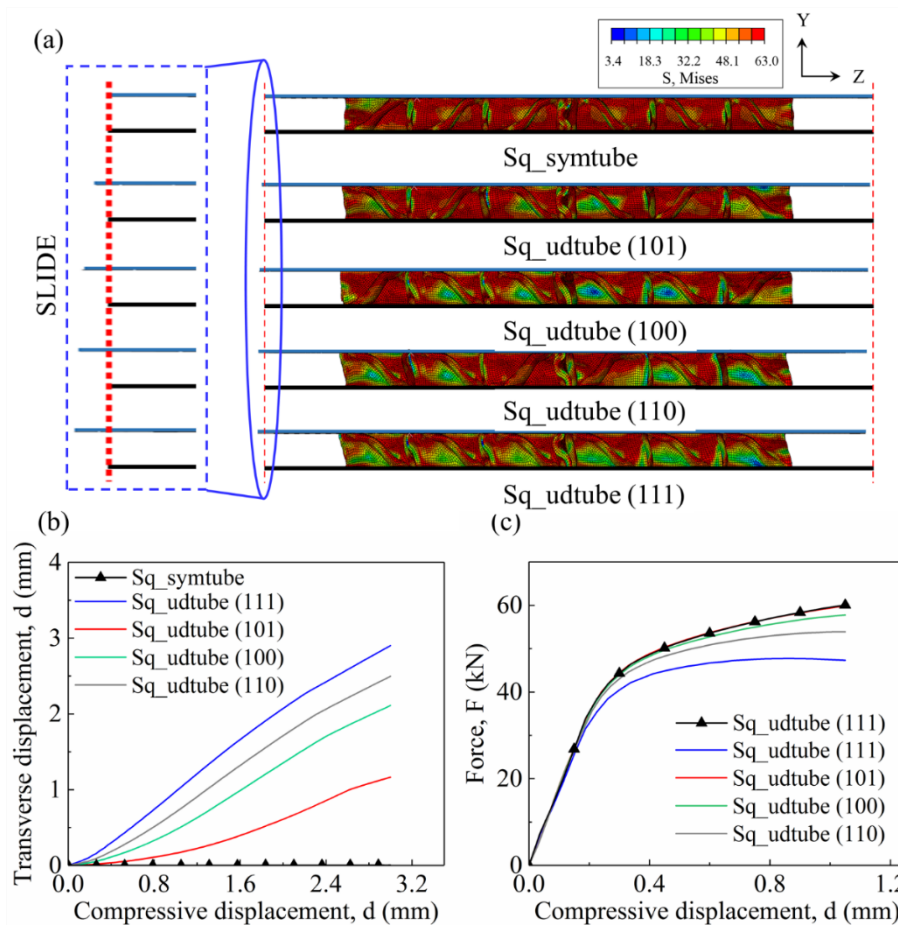


Figure 9



Please cite the article as: J Xu, Y Wu, L Wang, J Li, Y Yang, Y Tian, Z Gong, P Zhang, S Nutt, and S Yin ,
“Compressive properties of hollow lattice truss reinforced honeycombs (honeytubes) by additive manufacturing: patterning and tube alignment effects” *Matls & Design* 156 (2018) 446-457 DOI:
[10.1016/j.matdes.2018.07.019](https://doi.org/10.1016/j.matdes.2018.07.019)



Figure 10

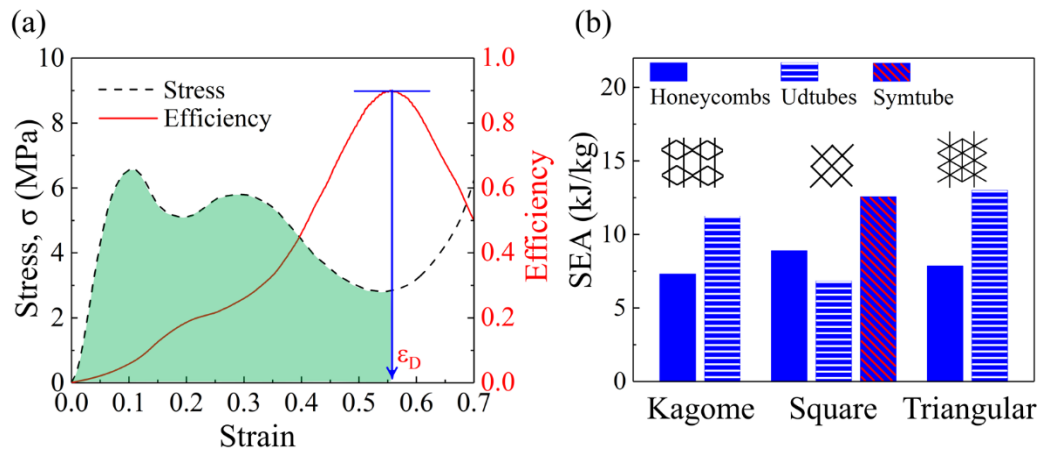


Figure 11

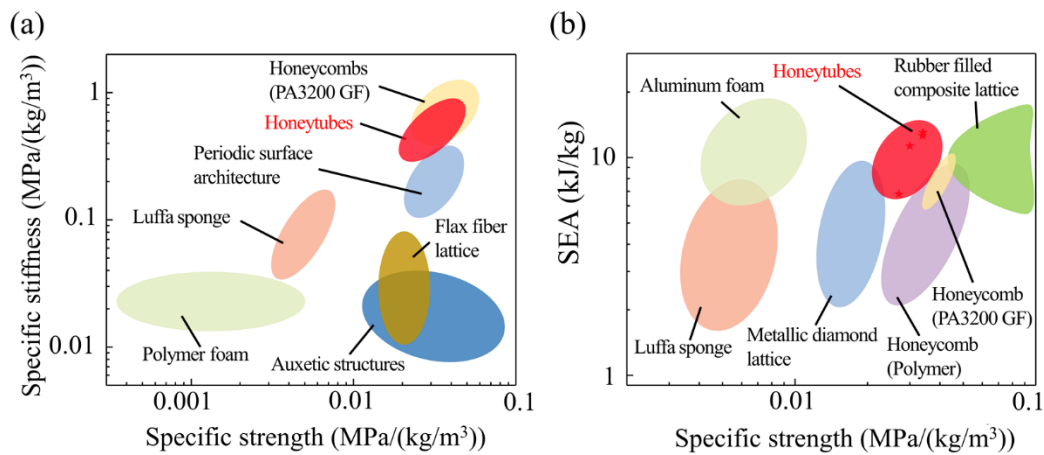
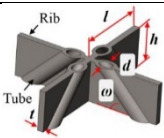


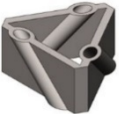
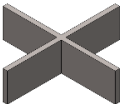



Figure 12

Please cite the article as: J Xu, Y Wu, L Wang, J Li, Y Yang, Y Tian, Z Gong, P Zhang, S Nutt, and S Yin ,
**“Compressive properties of hollow lattice truss reinforced honeycombs (honeytubes) by additive
 manufacturing: patterning and tube alignment effects”** *Matls & Design* 156 (2018) 446-457 DOI:
 10.1016/j.matdes.2018.07.019



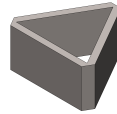
Table 1. Summary of geometries for honeytubes and the corresponding honeycombs.

| Specimen | Illustrations | h (mm) | t (mm) | d (mm) | ω (°) | l (mm) | Relative density (By Eq. 1) |
|---------------|-------------------------------------------------------------------------------------|-------------|-------------|-------------|-----------------|-------------|--------------------------------|
| Sq_symtube |  | | | | | | 0.175 |
| Sq_udtube |  | 10 | 1.5 | 4 | 45 | 18.6 | 0.175 |
| Kag_udtube |  | | | | | | 0.151 |
| Tri_udtube |  | | | | | | 0.303 |
| Sq_honeycomb |  | 10 | 1.5 | / | / | 18.6 | 0.161 |
| Kag_honeycomb |  | | | | | | 0.140 |

Please cite the article as: J Xu, Y Wu, L Wang, J Li, Y Yang, Y Tian, Z Gong, P Zhang, S Nutt, and S Yin ,
**“Compressive properties of hollow lattice truss reinforced honeycombs (honeytubes) by additive
 manufacturing: patterining and tube alignment effects”** *Matls & Design* 156 (2018) 446-457 DOI:
 10.1016/j.matdes.2018.07.019



Tri_honeycomb



0.279

Sq: square shaped honeycombs; Kag: Kagome shaped honeycombs; Tri: triangular shaped honeycombs ; symtube: symmetrically aligned hollow tubes; udtube: uni-directionally aligned hollow tubes in each strip of honeycombs.

Table 2. Summary of geometrical parameters employed in simulation.

| Models | Fixed parameters | | | Variables |
|------------|-------------------------|-------|-------|-----------|
| | ω ($^{\circ}$) | t/l | d/l | |
| Sq_udtube | 45 | / | 0.2 | 0.050 |
| Kag_udtube | | | | 0.083 |
| Tri_udtube | | | | 0.117 |
| Sq_symtube | | | | 0.150 |
| Sq_udtube | 60 | 0.05 | / | 0.183 |
| Kag_udtube | | | | 0.067 |
| Tri_udtube | | | | 0.133 |
| Sq_symtube | | | | 0.200 |
| Sq_udtube | / | 0.05 | 0.133 | 0.267 |
| Kag_udtube | | | | 30 |
| Tri_udtube | | | | 45 |
| Sq_symtube | | | | 60 |
| | | | | 75 |
| | | | | 90 |